*Korean J. Chem. Eng.*, **24**(2), 354-360 (2007)

# Characteristic modes and flow structure of non-premixed flame in humid-air combustion

**Gu Xin, Zang Shusheng[†] and Ge Bing**

School of Mechanical Engineering, Shanghai Jiao Tong University, Shanghai 200030, China
(*Received 30 August 2006 • accepted 21 October 2006*)

**Abstract**–An experimental study has been performed in order to determine the effect of humidity on the flow field and the flame stability limit in turbulent non-premixed flame. Two-dimensional Particle Image Velocimetry (PIV) measurements were made to quantify the velocity field, with and without steam injected. The results indicate the addition of steam decreases the recirculation flow and reduces the distance between the forward and aft stagnation points. The detailed stabilization regimes show that the critical fuel-to-air velocity ratios of the central fuel penetration in the humid air case are 16% to 22% lower, and the partially quenching limits are at least 25% lower. The decreased penetration limit is due to a reduction in momentum of the humid air. An analysis of flamelet concepts reveals that increased chemical reaction time leads to lower partially quenching limits in the humid air combustion.

Key words: Humid Air Combustion, Non-premixed Combustion, Recirculation Zone, Flamelet Concept

## INTRODUCTION

Environmental regulations regarding emissions of nitrogen oxide from combustor systems are becoming increasingly stringent worldwide. Many attempts to meet the $NO_x$ emission limit have been made [1-3]. It is known that combustor systems which rely on diffusion combustion can be stable over a wide range of operation conditions. The flame temperature, however, is rather high due to the creation of high-temperature stoichiometric interfaces, which leads to large $NO_x$ emissions. The steam-injected gas turbine (STIG) cycle and the humid air turbine (HAT) cycle are used as a means to meet severe $NO_x$ emission regulations on stationary gas turbines. One of the characteristics in these cycles is water or steam injected into combustors. Since water and steam have lower temperature and large heat capacity, its addition into the combustion field brings about the decrease in flame temperature [4]. The temperature decrease is very effective for suppression of thermal $NO_x$ formation [5-7]. Unfortunately, the flame stability is often adversely affected by the high efficiency and reduced $NO_x$ strategy. The flow characteristics and the flame structure with water or steam injected will be affected severely. Therefore, it is necessary to study the mechanism of the characteristic flow field and flame structure in humid air combustion.

Many studies of flame structure have been made to elucidate the basic combustion theory and mechanism [8-13], for example, flamelet structure and triple flame structure. Chen et al. [11] have investigated experimentally the combustion stabilization mechanisms for bluff-body stabilized non-premixed flame. The results obtained were that the flame appearances and the structures are basically classified into three stable types (recirculation zone flame, central jet dominated flame and jet-like flame) and two unstable types (partially quenching flame and lifted flame) before blowing-out. The air-to-fuel velocity ratio is the main controlling parameter. Similar flame structures were achieved by Esquiva-Dano et al. [12].

In recent years, particle image velocimetry (PIV) has become an important measurement technique allowing a better understanding of both reacting and non-reacting flows. Madsen and McCluskey [14] verified the accuracy and reliability of PIV measurements. Papadopoulos et al. [15] performed phase-locked measurements of the velocity field in the centerplane of an acoustically forced methane-air diffusion flame using PIV. Higuchi et al. [16] investigated the behavior of the leading-edge separating shear layer and its effect on the wake in water using both flow visualization and PIV techniques. Obi and Tokai [17] studied the flow around a pair of bluff bodies set in tandem. Braza et al. [18] analyzed the turbulence properties in unsteady flows around bluff body wakes. Yoshioka et al. [19] investigated experimentally the turbulent statistics of an unsteady separated flow by PIV.

The above discussion indicates the importance and feasibility for further understanding of the humid air flame aerodynamics and structure to allow robust design of a humid air combustor. The objective of this study is to examine the effect of humidity on the flow field and the flame stability in turbulent non-premixed flame. The flow structure in non-premixed flame behind a disk bluff-body are described and discussed via PIV measured results. The study focuses on developing gas turbine combustor design criteria for the Humid Air Turbine (HAT) cycle and providing a reliable database for code validation.

## EXPERIMENTAL DETAILS

### 1. Burner Description and Flow Condition

A schematic drawing of the burner and the PIV measurement field is shown in Fig. 1. The burner consisted of a circular disk bluff-body ($D_B$) 40 mm in diameter and a 4-mm diameter fuel jet ($D_j$) located in the center of the disc bluff-body. Methane was injected through the central fuel tube into annular air flow. The co-flow mixture of steam and air flowed through a 60 mm wind tunnel ($D_a$) and around the stagnation plate. The superheated steam generated by a

[†]To whom correspondence should be addressed.
E-mail: sszang@sjtu.edu.cn
[‡]This paper was presented at the 6[th] Korea-China Workshop on Clean Energy Technology held at Busan, Korea, July 4-7, 2006

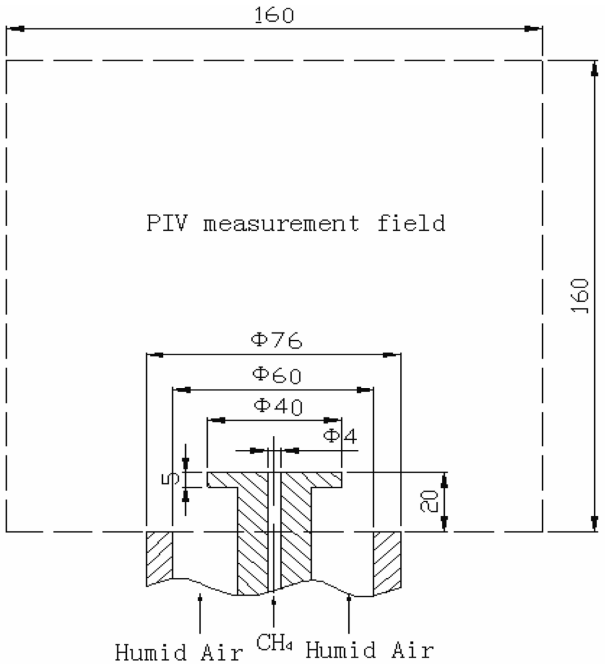


**Fig. 1. Nozzle structure and PIV measurement field.**

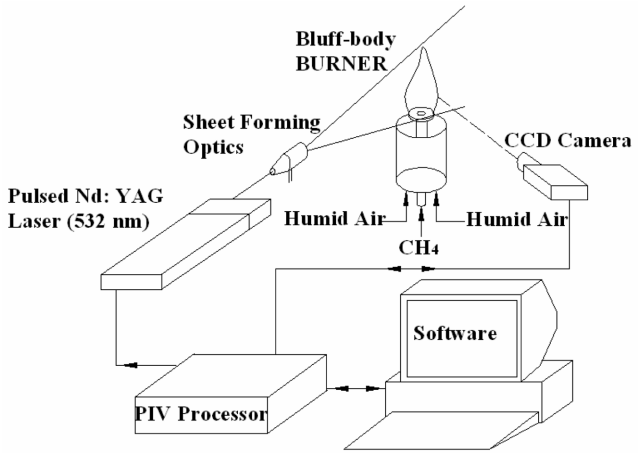


**Fig. 2. Schematic diagram of particle image velocimetry system for velocity measurements.**

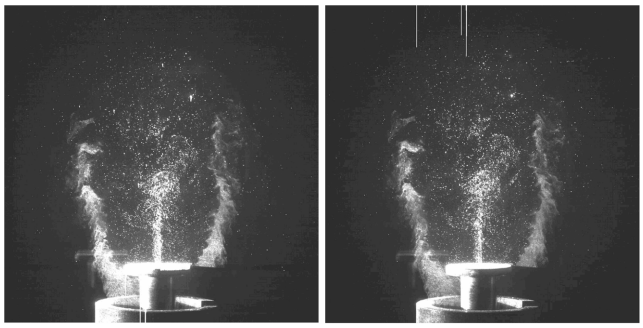

**Fig. 3. Double exposure particles photos for humid air combustion.**

**Table 1. Flame studies and their parameters**

| Flame No. | $V_f/V_a$ | $T_a$ (K) | $\Phi$ | d (g/kgDA) | $Re_f/Re_a$ |
|---|---|---|---|---|---|
| FN1 | 5/7.91 | 298 | 0.048 | 0 | 1087/10172 |
| FH1 | 5/7.91 | 337 | 0.06 | 200 | 1087/7633 |
| FN2 | 12.5/7.91 | 298 | 0.12 | 0 | 2696/10172 |
| FH2 | 12.5/7.91 | 337 | 0.15 | 200 | 2696/7633 |

steam generator was mixed with the dry air before entering the combustor. The steam (d) was controlled constant at 200 g/kg (dry air) and the steam content in the humid air was as much as 24% by volume. In order to achieve accurate evolution and characterization of the stabilization regimes, a wide range of fuel jet velocities were presented, from 5 m/s to 45 m/s with every 2.5 m/s break, when the co-flow air or humid air was kept at exit velocities of 3.72 m/s, 5.29 m/s, 7.91 m/s, 9.78 m/s and 12.5 m/s, respectively. The addition of steam will severely affect the characteristic velocity field. However, to illustrate the influence of humid air on the velocity structures, only the experimental cases in Table 1 will be presented.

## 2. Particle Image Velocimetry

A schematic diagram of two-dimensional Particle Image Velocimetry (Dantec) for carrying out velocity measurements is shown in Fig. 2. The PIV system consists of a laser illumination source, digital imaging device, and dedicated hardware and software for data analysis. The illumination source is a double pulsed Nd: YAG laser operating at a wavelength of 532 nm (200 mJ per pulse). Particle image pairs were accomplished via an 8-bit double-frame CCD camera (Kodak ES 1.0) having a resolution of 1,008×1,018 pixels. A bandpass filter centered at 532 nm (±10 nm) was placed in front of the camera lens to reduce flame luminosity effects on the acquired images. The field of view was about 160 mm×160 mm of the flow region. The velocity vectors were evaluated by cross-correlation methods by using an interrogation area of 64×64 pixels with a 50% overlap, which thus gave 30 vectors in each direction. Erroneous vectors were eliminated by applying an average filter. Of course, the size of the interrogation window effectively limits the size of the vortex structures captured. For determining the mean velocity profile precisely, a series of 200 of instantaneous measurements were statistically averaged [20] in each operating mode.

The submicron MgO, which was supplied by a fluidized bed seeder, served as seeding particles in the fuel jet and co-flow air stream. The co-flow humid air does not need seeding particles due to the added steam, as shown in the photos in Fig. 3. The seeders were equipped with bypasses to allow control of the seeding density. The zero-velocity biasing can be minimized by ensuring that there are always at least five seeding particles within each interrogation area.

Major source of uncertainty of PIV measurement is considered to be the effect of velocity gradient (Keane [21]). Uncertainty of the PIV velocity measurement was estimated ±10% for the mean value with a 95% confidence interval.

## RESULTS AND DISCUSSIONS

### 1. Flame Appearances for Humid Air Combustion

Wide variations in flame shape have been observed for both humid and non-humid cases. The structures were studied both visually, through photography and with the velocity results obtained by PIV

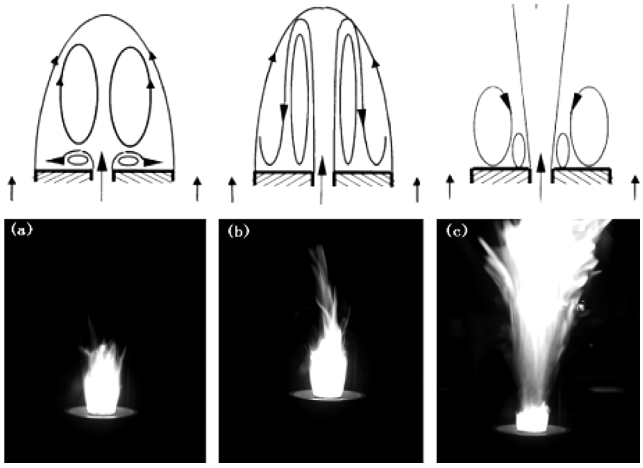


**Fig. 4. Flame appearances for humid air combustion, (a) recirculation zone flame, (b) transition flame, (c) central-jet dominated flame.**

in this paper. The visual appearance of flame in the humid air combustion is similar to that observed in the non-humid air case. Three stable modes, which are recirculation zone flame, transition flame and central jet dominated flame, respectively, can be observed. At higher annular air velocities ($V_a \geq 3$ m/s), the jet-like flame and lifted flame mentioned above cannot be formed. These flame shapes are primarily a result of the effect of the fuel-to-air velocity ratio and the humidity level.

An example of three stable flame structures is presented in Fig. 4 for the humid air case. Two typical flame modes, recirculation zone flame and central jet dominated flame, can be distinguished from the direct visual features of the flame. It was visually observed that the recirculation zone flame is relatively shorter in shape as shown in Fig. 4a. For a long central jet dominated flame, a blue neck is formed immediately downstream of the apex of the recirculation bubble. The flame does not shift into central jet dominated flame until most of the fuel jet can penetrate the recirculation bubble to reach further downstream and be reignited, as shown in Fig. 4c. The transition flame is the transitional status between recirculation zone flame and central-jet dominated flame, at which most of the fuel is consumed inside the recirculation bubble and only a little residual fuel penetrates the recirculation zone as illustrated in Fig. 4b.

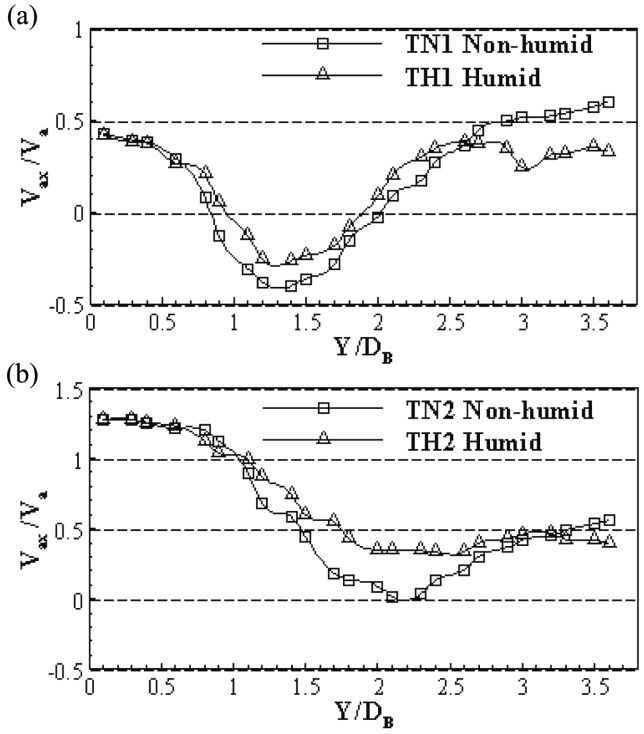


**Fig. 6. Axial mean velocity profiles on the centerline, (a) $\gamma$=0.63, (b) $\gamma$=1.58.**

The use of PIV to determine flow structure has become more popular in the last few years. Fig. 5 presents the mean velocity vectors for the humid air flame in the selected cases of the fuel-to-air velocity ratios ($\gamma$) are 0.8, 1.98 and 2.99, respectively. Note that the velocity vectors correspond to the observed photographic images in Fig. 4, respectively. It is clear that the fuel in Fig. 5a is obstructed from the reverse air stream and can only reach a height of 36 mm. As a result, the central fuel can be consumed completely inside the recirculation bubble to form recirculation zone flame. In addition, for the $\gamma$=1.98 case, the central fuel jet can reach the apex area of the recirculation zone to form neither recirculation flame nor central jet dominated flame but transition flame. When most of the central fuel penetrates the recirculation bubble to be burned in the further downstream of recirculation bubble, the classical central jet dominated flame is formed, at which the velocity values on the center-

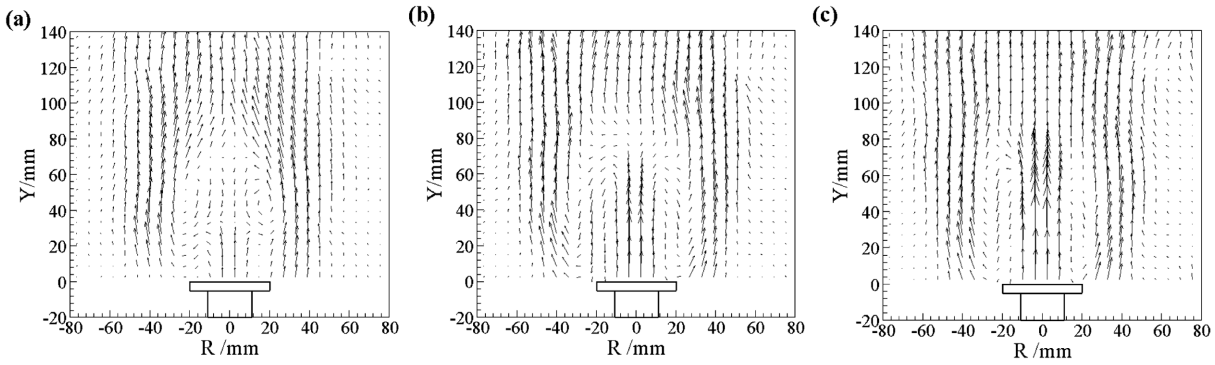


**Fig. 5. Velocity vectors in humid air combustion for different flame appearances, (a) recirculation zone flame, (b) transition flame, (c) central-jet dominated flame.**

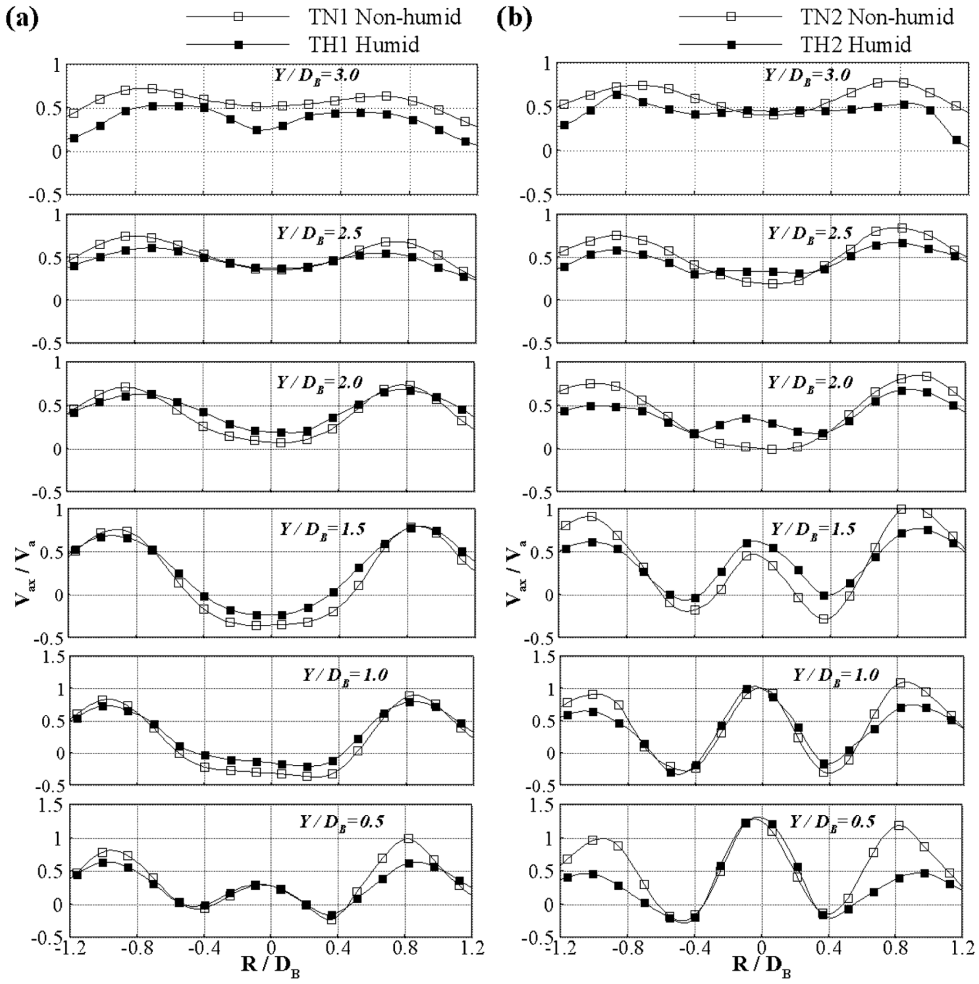


**Fig. 7. Axial mean velocity profiles in axial sections, (a) $\gamma$=0.63, (b) $\gamma$=1.58.**

line remain consistently positive.

### 3. Effect of Humid Air on the Characteristic Velocity Fields

The centerline evolutions of the mean axial velocity for both humid air and non-humid air cases are presented in Fig. 6. Note that in this and the next figure, dimensionless scales for velocities and lengths are the annular air velocity at nozzle exit $V_a$ and the bluff-body diameter $D_B$. In contrast, the dimensionless axial velocities on the centerline are somewhat higher in the humid air case (FH1 and FH2) than that observed in the non-humid air case (FN1 and FN2). The momentum of the fuel jet for the flame FN1 and FH1 is too weak to overcome that of the reverse air flow at a velocity ratio of 0.63. The fuel mass will be therefore retained behind the bluff-body and consumed completely to form a recirculation zone flame. It can be observed that two stagnation points on the centerline exist within the recirculation bubble. The two stagnation points are, respectively, aft (air) and forward (fuel) stagnation points where the axial velocities on the centerline are just equal to zero [13]. As can be seen in Fig. 6a, the distance between the two stagnation points in the humid air case (TH1) decreases due to the nearer forward stagnation point and the farther aft stagnation point, which implies a reduced recirculation zone. It is necessary to note that only one stagnation point exists on the centerline for the conventional non-humid air flame (TN2), but no stagnation point for the humid air combustion (TH2) at velocity ratio close to 1.58. One stagnation point indicates that the fuel jet can just reach the apex area of the recirculation zone, and the fuel-jet can even penetrate the recirculation bubble if the fuel-jet velocity is a bit higher. The comparison shows that the recirculation zone shortens and the fuel-jet penetrates recirculation zone more easily in the humid air combustion.

Profiles of mean axial velocity on several axial sections for the humid and non-humid air flame are provided in Fig. 7. Hedman [22] examined the zero axial velocity and zero radial velocity contours to help define recirculation regions. As can be seen, the reverse flow vanishing at $Y/D_B$=2.0 and the further downstream indicates the length of the recirculation zone is nearly two times the diameter of the bluff-body. A slight reverse flow happens near the centerline at $Y/D_B$=1.0 and $Y/D_B$=1.5 in the case of $\gamma$=0.63, which indicates the central-jet cannot penetrate the recirculation bubble. However, when $\gamma$=1.58, the reverse flow occurs at the region of $R/D_B$=0.4, which implies the air recirculation vortex is separated into two symmetrical independent vortices. A comparison between Fig. 7a and 7b shows the velocity ratio is the main factor to affect the flow structure. The comparison of the humid and non-humid cases indicates that in the vicinity of nozzle exit, the velocity near the centerline in the humid air combustion is maintained identically with the velocity in conventional non-humid combustion. However,

far from the nozzle exit to farther downstream at $Y/D_B$=1.5 and 2.0, the velocity on the centerline in the humid air case exceeds the velocity in the non-humid air case. In addition, it is also clear that the annular humid airflow induces lower axial velocities and velocity gradients in all axial sections as shown in Fig. 7. The lower annular air flow leads to a comparatively weak flow recirculation, which causes an easier transformation from the recirculation flame to the central-jet dominated flame for the humid air flame.

To provide more insight into the effect of added steam on the flame structure, the streamlines in humid (TH2) and non-humid (TN2) air flame are illustrated in Fig. 8. As can be seen, the velocity field has a symmetry feature. Two kinds of vortices (air vortex and fuel vortex) are symmetric along the centerline of the bluff-body, respectively. The point at which the fuel vortex meets the reverse flow air vortex is the region of heat and mass exchanged. It can be observed that the flow fields are remarkably different in the two cases though the humid air flame has the same inlet fuel and air velocities as the non-humid air flame. In the humid air combustion, most of the fuel can penetrate the recirculation bubble to farther downstream. In the non-humid air case, however, the fuel jet could not penetrate the recirculation zone. The result indicates the humid air flame is in the complete central-jet dominated flame, but the non-humid air flame is still the recirculation zone status.

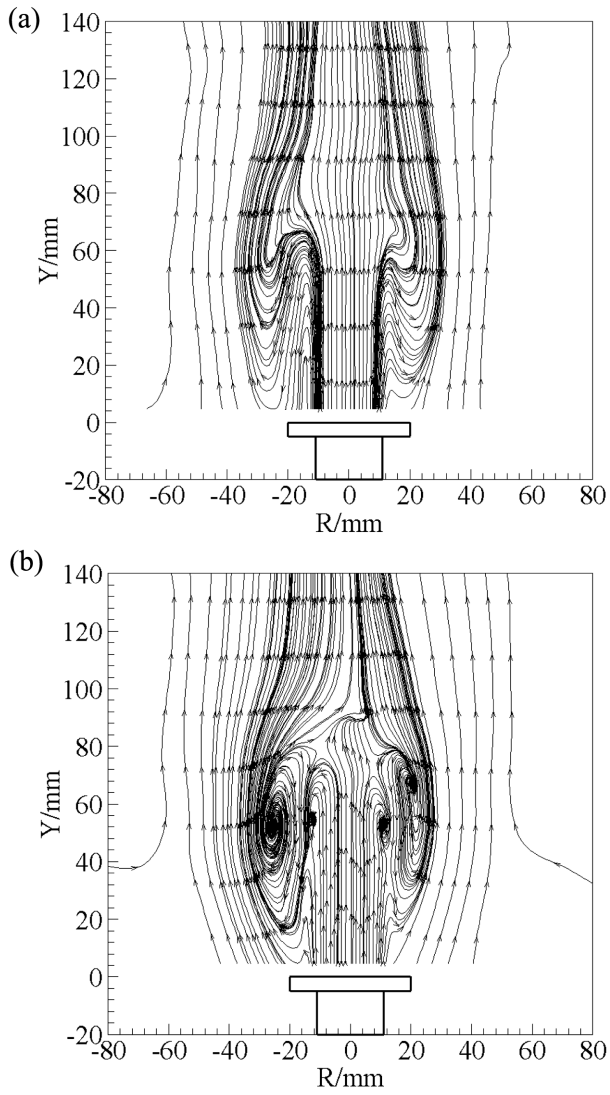


**Fig. 8. Streamlines for the humid and non-humid air flame: (a) humid air flame (TH2), (b) non-humid air flame (TN2).**

## 4. Stabilization of Humid Air Flame

In general, the flame can be stable with relative lower central fuel velocity. Flame characteristic structures are strongly related to the fuel-to-air velocity ratio which directly affects the vortex structure behind the bluff-body. As noted above, the fuel-to-air velocity ratio is an important parameter to control flame stabilization. To this end, the PIV velocities fields are measured over a wide range of values of fuel velocities with fixed annular air velocities. The minimal axial velocities variations on the centerline against the fuel-to-air velocity ratios are obtained as shown in Fig. 9. The penetration limits

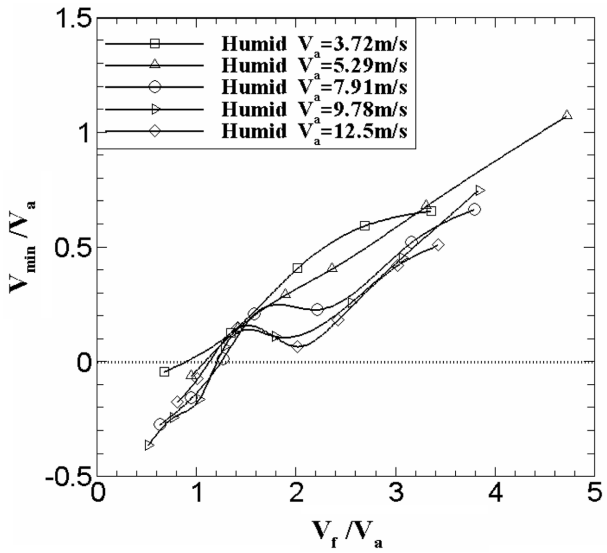


**Fig. 9. The minimal axial velocity variations on the centerline for humid air combustion.**

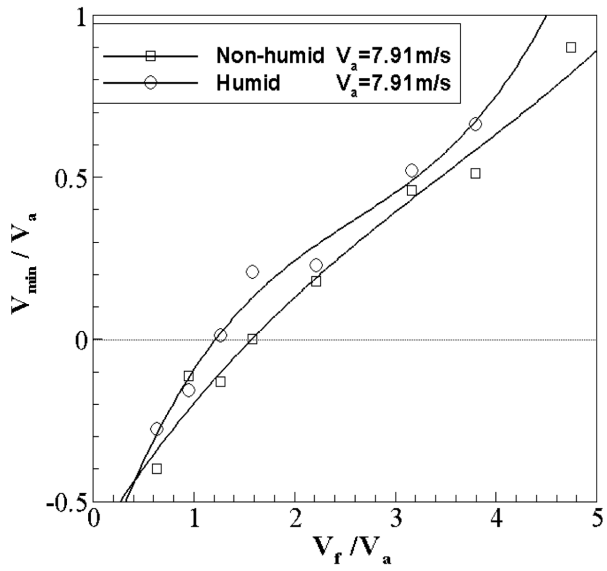


**Fig. 10. The comparison of minimal axial velocities on the centerline for humid and non-humid air flame.**

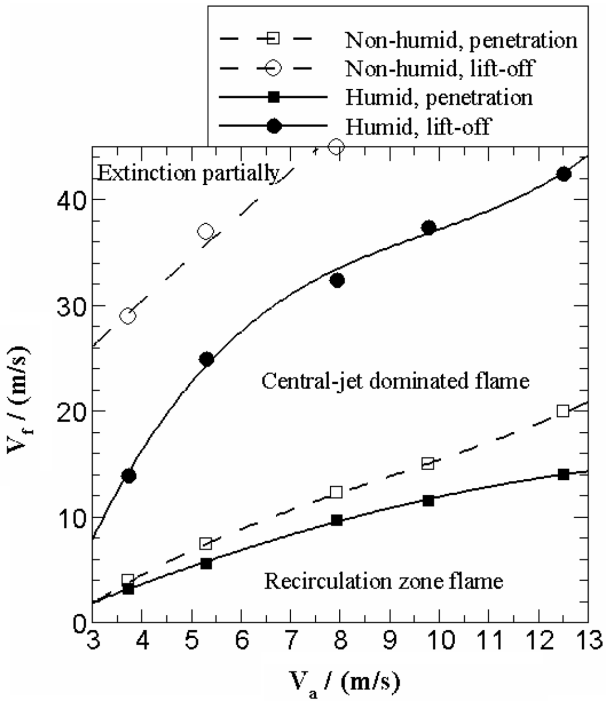


**Fig. 11. Stabilization regimes for the humid and non-humid air flame.**

($\gamma_p$), which are used to separate recirculation zone flame and central-jet dominated flame, are obtained when the minimal dimensionless axial velocities ($V_{min}/V_a$) are zero. The values of $\gamma_p$ for humid air flame vary from 0.9 to 1.25 as can be seen in Fig. 9. Fig. 10 presents a comparison of minimal axial velocities on the centerline in the humid and non-humid air cases. It is clear that the penetration limit in the non-humid air flame is 1.6, instead of the value 1.25 in the humid air case. The $\gamma_p$-limits in the humid case are about 20% lower than that of non-humid case.

Fig. 11 presents a comparison of stabilization regimes for the humid and non-humid air flames. The limits for partially quenching (lift-off) in the blue neck area downstream of the recirculation zone are specified by direct visualization. As the ratio of fuel-to-air is increased, the flame will shift into central-jet dominated flame from recirculation zone flame, even into the unstable flame mode, partially quenching flame. The transition flame is the transitional status between recirculation zone flame and central-jet dominated flame, which can be observed around the penetration limits. The partially quenching flame is a kind of unstable flame mode, and with increasing velocity ratio of the fuel-to-air, the flame is likely to blow out suddenly. A more likely and realistic view for explaining the partial quenching is that the mixing time scale over the chemical time scale in the close downstream region of recirculation zone leads flame to extinguish partially [23]. The flame may also be reignited further downstream where turbulent mixing rates are abated. The comparison shows that although the flame modes of the humid air combustion are similar to that observed in the non-humid air case, the critical fuel velocities ($V_f$) for the humid air flame are much lower under the fixed annular air velocity ($V_a$). In other words, when conventional non-humid air combustion flame is in the region of recirculation zone flame, the humid air flame may transit to central jet dominated status. Moreover, when the partial quenching occurs in the humid air case, the conventional non-humid flame may be still in the central-jet dominated flame. Therefore, the result clearly shows that the flame with steam added is unstable.

There are both physical and chemical effects on combustion phenomena with the addition of steam. Reduction in momentum of the humid air is a main fluid dynamic reason for unstable flame. The annular airflow induces lower velocities in the humid air case through same inlet velocities as discussed in Fig. 7, which will result in a decrease in momentum of the humid air. Moreover, the molecular weight of the humid air is only 26.3 g/mole rather than 28.97 g/mole for the dry air, and thus the lower molecular weight of humid air causes further reduction in the momentum. As a result, flow recirculation will be decrease, which will cause the fuel flow at fixed velocity to penetrate the recirculation zone more easily. The $\gamma_p$-limits of penetration, as proposed by Chen et al. [11] should be multiplied by $(\rho_f/\rho_a)^{0.5}$. Esquiva-Dano et al. [12] point to the fact that the characteristic flame modes should be controlled by mass flux ratio. Furthermore, it is important to note that the molecular kinematic viscosity is increased by 25% with steam added. The increased viscosity may explain the fact that the annular humid air induced lower velocity, due to which the recirculation strength will be reduced. Therefore, the penetration occurs at a lower fuel-to-air velocity ratio in the humid case. Similarly, the oxygen content of the humid air is only 15.9% instead of normal 21% in typical dry air. The overall equivalence ratio ($\Phi$) in humid air combustion is increased by 25% over the corresponding dry air equivalence ratio. The increasing equivalence ratio and the dilution effect of steam result in a lower O-atom concentration, which will decrease the chemical reaction rate. The flamelet concepts suggest that the extinction occurs when the Damköhler second similarity number is less than some critical value. The increased rate of heat transfer to humid air can lower the flame temperature, which also leads to an increase in the actual chemical reaction time ($\tau_{ch}$) [24]. Therefore, the increased chemical reaction time may be one plausible reason for the lower partially quenching limit in the humid air flame.

## CONCLUSIONS

An aerodynamic flow field and stabilization for both humid air and non-humid flames are observed based on two-dimensional PIV in this work. The humid air flame modes are similar to that observed in the non-humid air. The flame can be classified into three stable modes: recirculation zone flame, transition flame and central jet dominated flame. The fuel-to-air velocity ratio is the main parameter to control the flame modes. A comparison between the humid air and non-humid air combustion indicates that the recirculation zone shortens and the flow recirculation decreases with steam added, which brings about an unstable humid air flame. In addition, the stabilization regimes reveal that both the penetration limits and the partially quenching limits decrease in the humid air case. The reduction in momentum of the humid air is the main reason for explaining the reduced penetration limits. The lower partially quenching limits are due to the decrease of Damköhler number resulting from the increasing chemical reaction time. The quantitative experimental data in humid air combustion by visualization PIV technique can become the references for future simulation.

## ACKNOWLEDGMENT

The authors gratefully acknowledge the State Key Fundamental Research Program of China (through Research Grant no. G1999022303) for the financial support.

## REFERENCES

1. D.-H. Chung, J.-B Yang, D.-S Noh and W.-B Kim, *Korean J. Chem. Eng.*, **16**, 489 (1999).
2. K.-W. Cho, H.-S. Park and Y.-K. Lee, *Korean J. Chem. Eng.*, **10**, 140 (1993).
3. J. Chaouki, D. Klvana and C. Guy, *Korean J. Chem. Eng.*, **16**, 494 (1999).
4. A. Katoh, M. Shinoda, K. Kitagawa and A. K. Gupta, *J. Eng. Gas Turb. Power*, **128**, 8 (2006).
5. A. Bhargava, M. Colket, W. Sowa, K. Casleton and D. Maloney, *J. Eng. Gas Turb. Power*, **122**, 405 (2000).
6. F. L. Dryer, *in 16th Symposium (International) on Combustion*, The Combustion Institute, Pittsburgh, 279 (1976).
7. T. Miyauchi, Y. Mori, and T. Yamaguchi, *in 18th Symposium (International) on Combustion*, The Combustion Institute, Pittsburgh, 43 (1980).
8. S. S. Vakil and K. A. Thole, *J. Eng. Gas Turb. Power*, **127**, 257 (2005).
9. K. Midgley, A. Spencer and J. J. McGuirk, *J. Eng. Gas Turb. Power*, **127**, 755 (2005).
10. B. B. Dally, A. R. Masri, R. S. Barlow and G. J. Fiechtner, *Combust. Flame*, **114**, 119 (1998).
11. Y. C. Chen, C. C. Chang, K. L. Pan and J. T. Yang, *Combust. Flame*, **115**, 51 (1998).
12. I. Esquiva-Dano, H. T. Nguyen and D. Escudie, *Combust. Flame*, **127**, 2167 (2001).
13. R. F. Huang, J. T. Yang and G. L. Lee, *Combust. Flame*, **108**, 9 (1997).
14. A. H. Madsen and D. R. McCluskey, *in 7th International Symposium on the Application of Laser Techniques to Fluid Mechanics*, Lisbon, Portugal Springer Verlag (1994).
15. G. Papadopoulos, R. A. Bryant and W. M. Pitts, *in 2nd Joint Meeting of the US Sections of the Combustion Institute*, Oakland, CA (2001).
16. H. Higuchi, P. van Langen, H. Sawada and C. E. Tinney, *J. Fluid Struct.*, **22**, 949 (2006).
17. S. Obi and N. Tokai, *Int. J. Heat Fluid Fl.*, **27**, 768 (2006).
18. M. Braza, R. Perrina and Y. Hoarau, *J. Fluid Struct.*, **22**, 757 (2006).
19. S. Yoshioka, S. Obi and S. Masuda, *Int. J. Heat Fluid Fl.*, **22**, 393 (2001).
20. C. D. Meinhart, S. T. Wereley and J. G. Santiago, *J. Fluids Eng.*, **122**, 285 (2000)
21. R. D. Keane and R. J. Adrian, *Meas. Sci. Technol.*, **1**, 1202 (1990).
22. P. O. Hedman, T. H. Fletcher, D. V. Flores, S. G. Graham, J. K. Haslam, R. L. Murray and G. W. Timothy, *J. Eng. Gas Turb. Power*, **127**, 724 (2005).
23. A. R. Masri, R. W. Dibble and R. S. Barlow, *Prog. Energy Combust. Sci.*, **22**, 307 (1996).
24. F. A. Williams, *Prog. Energy Combust. Sci.*, **26**, 657 (2000).